

Additive-free low temperature sintering of amorphous Si B C powders derived from boron-modified polycarbosilanes: Toward the design of SiC with tunable mechanical, electrical and thermal properties

Maxime Balestrat, Emanoelle Diz Acosta, Ondrej Hanzel, Nicolas Tessier-Doyen, Ricardo J. Machado, Pavol Šajgalík, Zoltán Lenčéš, Samuel Bernard

▶ **To cite this version:**

Maxime Balestrat, Emanoelle Diz Acosta, Ondrej Hanzel, Nicolas Tessier-Doyen, Ricardo J. Machado, et al.. Additive-free low temperature sintering of amorphous Si B C powders derived from boron-modified polycarbosilanes: Toward the design of SiC with tunable mechanical, electrical and thermal properties. Journal of the European Ceramic Society, 2020, 40, pp.2604-2612. 10.1016/j.jeurceramsoc.2019.12.037 . hal-02474847

HAL Id: hal-02474847
https://unilim.hal.science/hal-02474847

Submitted on 21 Dec 2020

HAL is a multi-disciplinary open access archive for the deposit and dissemination of scientific research documents, whether they are published or not. The documents may come from teaching and research institutions in France or abroad, or from public or private research centers.

L'archive ouverte pluridisciplinaire **HAL**, est destinée au dépôt et à la diffusion de documents scientifiques de niveau recherche, publiés ou non, émanant des établissements d'enseignement et de recherche français ou étrangers, des laboratoires publics ou privés.

Additive-free low temperature sintering of amorphous Si-B-C powders derived from boron-modified polycarbosilanes: Toward the design of SiC with tunable mechanical, electrical and thermal properties

Maxime Balestrat[a], Emanoelle Diz Acosta[a,b], Ondrej Hanzel[c], Nicolas Tessier-Doyen[a], Ricardo Machado[b], Pavol Šajgalík[c], Zoltán Lenčéš[c], Samuel Bernard[a,*]

[a] Univ. Limoges, CNRS, IRCER, UMR 7315, F-87000, Limoges, France
[b] Chemical Engineering, Federal University of Santa Catarina, 88010-970, Florianópolis, Brazil
[c] Institute of Inorganic Chemistry, Slovak Academy of Sciences, 84536, Bratislava, Slovakia

A B S T R A C T

Additive-free SiC ceramics are prepared from polymer-derived powders with Si, C and B elements homo-geneously distributed on the atomic level by rapid hot-pressing at 1750 °C and 1800 °C under argon and a load of 50 MPa. As-sintered samples display a Vickers hardness in the range of 9.6 ± 0.5 GPa–17.3 ± 1.9 GPa and an elastic modulus varying from 137 ± 3.4 GPa to 239 ± 6 GPa, both depending on the sample phase composition, crystallinity and porosity. Accordingly, the electrical conductivity changes from 340 to 3900 S/m whereas the thermal conductivity varies from 17.7 to 45.1 W/m K as a function of these characteristics. Thus, we demon-strated that a polycarbosilane containing 0.7 wt.% of boron could produce boron-doped SiC powders that de-monstrate tailored sinterability at temperatures as low as 1750 °C to form nearly dense SiC ceramics with adjusted hardness, Young's modulus, electrical and thermal conductivities.

1. Introduction

Silicon carbide (SiC), a highly covalent engineering ceramic with high strength and decomposition temperature, high oxidation/corro-sion and thermal shock resistance and low coefficient of friction, is conventionally used in high-end applications where high-temperature stability, chemical resistance and mechanical reliability are required.

SiC ceramics for high temperature applications usually contain a small content of sintering additives (e.g., boron (B ≤ 0.3 wt.%), carbon (C 3 wt.%)) [1,2] to activate the powder and promote their sintering at high temperatures (T_S > 2000 °C) and under high pressure (p ≥ 30 MPa). Lower sintering temperatures (1750 °C–1850 °C) can be applied for the preparation of dense SiC ceramics by liquid phase sintering, when higher content of sintering additives (4–10 wt.%) like Al_2O_3, rare-earth oxides, or nitrides (AlN) are used [3]. In the case of "solid state sintering" of SiC with C and B additives, carbon inhibits the ineffective mass transport while boron favours diffusion and hence the densifica-tion of SiC ceramics [1,2]. However, there is still a number of issues limiting the commercial deployment of SiC ceramics including the homogeneous distribution of the sintering aids distribution in the SiC matrix, the control of the density and microstructure of the sintered bodies and the very high temperature needed to sinter raw powders [3,4].

In order to overlap these limitations, a chemical approach based on well-defined single-source precursors offering precise control over chemical compositions, microstructure and low processing temperature has been exploited in the present work. In particular, we investigated the polymer derived ceramics (PDCs) route as a convenient precursor-based approach to prepare the raw powders to be sintered. The PDCs method [5–15] is based on the synthesis of a preceramic polymer as a ceramic precursor and the thermo-chemical conversion of the latter into an amorphous ceramic. Optionally, an annealing process can be per-formed to crystallize the amorphous ceramics. The PDCs route also allows an easy polymer shaping (prior to pyrolysis) to produce thin ceramic parts or complex architectures such as fibers, coatings, dense or porous monoliths, printed 3D structures, etc. [16–21]. As an illustration, polymer-derived SiC can be produced in the form of nearly dense material by direct pyrolysis of a polymeric green compact obtained by warm pressing of the polymeric powder [22–25]. However, there are critical problems to take into consideration when using this route to prepare fully dense components such as the gas release or crystal-lization (if required) of amorphous phase during the polymer-to-

* Corresponding author.
E-mail address: samuel.bernard@unilim.fr (S. Bernard).

ceramic conversion. This typically leads to pore formation (evolving gases) and large volume shrinkage (phase segregation, crystallization) accompanied by the formation of large defects such as cracks or pores. Alternative strategies are based on the use of preceramic polymers as binders (up to 30 wt.%) [26–29] or on direct preparation of ceramic powders from tailor-made preceramic polymers to be sintered using the conventional way of sintering [30–34]. The sintering of ceramic pow-ders derived from polymers is really attractive to design dense cera-mics, especially if the powders exhibit a complex and tailored compo-sition made of three or more elements which cannot be prepared by the conventional ceramic powder technology [33,31–34]. However, when it comes to SiC, we still meet the same problems of sintering: a high temperature of sintering is usually required to densify the ceramics and sintering aids are usually applied [35,36]. As an illustration, the spark plasma sintering (SPS) of polycarbosilane-derived SiC powders requires very high sintering temperatures (2100−2200 °C) to consolidate the powders and produce sintered ceramics (95–96 % of T.D.) with Vickers hardness of 25 GPa [35]. Delobel et al. [36] applied the high energy ball milling for the activation of sintering of pyrolysed precursor. Al-though lower sintering temperature could be used for the sintering of powder, the sintered SiC body was contaminated with alumina, as the powder was milled in alumina jar. It is known that alumina is dele-terious to the high-temperature mechanical properties of SiC ceramics. Thus, there are still several key issues related to the existing approaches to sinter SiC which limit its large-scale application for enhanced system engineering. To face these issues, amorphous powders consisting of Si linked to C and homogeneously distributed sintering aids (i.e., B and free C) on atomic level have been prepared to be sintered by field as-sisted sintering technology (rapid hot-pressing, RHP) in this work. This approach should offer a structural and compositional homogeneity in the materials as well as a low temperature of sintering because of the synthesis of an appropriate polymeric precursor containing all the elements, i.e., Si, B and C, mixed at molecular scale. Allylhy-dridopolycarbosilane (AHPCS) [37–40] precursor has been selected for this purpose. It contains allyl groups that can be used to integrate ad-ditional elements like boron [41–43]. In our previous work [43], we demonstrated the possibility to tailor the boron and carbon contents in SiC powders when produced from boron-modified AHPCS. To our knowledge, the sintering of powders derived from boron-modified polycarbosilane has not been investigated yet, although it can demon-strate substantial interests in terms of sintering conditions and perfor-mance compared to both the sintering of SiC powders derived from polycarbosilane and sintering of commercially available SiC powders with sintering aids

Herein, we report on the sintering of boron-doped SiC powders derived from boron-modified AHPCS by RHP at relatively low tem-perature (T ≤ 1800 °C). The microstructure, hardness, Young's mod-ulus, electrical and thermal conductivities of prepared SiC ceramics are reported and discussed.

2. Experimental procedure

2.1. Preparation of powders and dense samples

Allylhydridopolycarbosilane (AHPCS labeled SMP-10, Starfire Systems® Incorporation, New York, USA), with a density of 0.998 g cm^{-3} was used as-received. Extra dry toluene (99.85 %) was obtained from Acros Organics. Borane dimethylsulfide BH_3 $S(CH_3)_2$ solution (2.0 M of BDMS complex in toluene) was obtained from Acros Organics.

The synthesis of boron-modified allylhydridopolycarbosilanes la-belled as AHPCSB60 and AHPCSB30 (60 and 30 being the Si:B atomic ratio (or AHPCS (its monomeric unit):BDMS molar ratio) fixed during the polymer synthesis) was carried out in a purified argon atmosphere passing through successive columns of catalysts and phosphorus pent-oxide by means of standard Schlenk techniques. The glassware was stored in an oven at 90 °C overnight before being assembled and pumped under vacuum for 30 min and then filled with argon. The powders were synthesized by reaction between AHPCS and BDMS ac-cording to our previous report [43]. The manipulation of polymers (for characterization and pyrolysis) was made inside an argon-filled glove box (Jacomex, Campus-type; O_2 and H_2O concentrations kept at ≤ 0.1 ppm and ≤ 0.8 ppm, respectively). As-synthesized polymers were ground in an agate mortar in the glove-box, then placed in alumina boats to be introduced in specially designed tubes to be transferred under argon flow into a silica tube inserted in a horizontal furnace (Carbolite BGHA12/450B). The tube was evacuated (0.1 mbar) and refilled with argon (99.995 %) to atmospheric pressure. Subsequently, the samples were subjected to a cycle of ramping of 5 °C/min to 800 °C with a dwell time for 2 h. A constant flow of argon was passed through the tube during the pyrolysis cycle. Powders are depicted as SiBC60 and SiBC30 obtained from AHPCSB60 and AHPCSB30 precursors, respec-tively.

The synthesized powders were milled in a vibrational agate mill for 2 h. The milled powders were poured into a graphite die (Ø 20 mm) lined with flexible graphite foil to prevent the direct contact between the sample and graphite die. The densification was performed in DSP 507 rapid hot-press (Dr. Fritsch GmbH, Germany) with non-pulsing current in argon atmosphere at 1750 °C or 1800 °C for 15 min under a uniaxial pressure of 50 MPa. The heating and cooling rates were 100 °C/min and 15 °C/min, respectively. Four pellet-shape specimens (ap-prox. 20 mm in diameter) with a thickness of 2.5 mm have been produced according to the Si:B atomic ratio (i.e., 30 and 60) fixed at molecular scale and the sintering temperature (i.e., 1750 °C and 1800 °C). The samples are labelled as follows: SiBC60_17, SiBC60_18, SiBC30_17, SiBC30_18 (17 and 18 being the first numbers of the tem-perature at which the sample were sintered: 17 for 1750 °C and 18 for 1800 °C). The overall flow chart of the process is shown in Fig. 1.

2.2. Material characterization

The AHPCSB60 and AHPCSB30 samples were characterized in de-tails in our previous report [43]. The phase composition of SiBC60 and SiBC30 samples and derived sintered samples was determined by XRD analysis (Bruker AXS D8 Discover, CuKα dariation). The scans were performed in the range of 2θ 20°; 90° with a step of 0.015° and an exposure time of 0.7 s. The diffraction patterns were analyzed using the Diffrac + EVA software with the JCPDS-ICDD database. The Raman spectra of the powders were recorded at room temperature using an InVia reflex Raman spectrometer (Renishaw, United Kingdom) equipped with a laser diode (λ =785 nm) in a backscattering geometry using a 100× objective lens and calibrated to pure Si. The spectra were measured in the range of 50–2030 cm^{-1}. The morphology of sintered samples was by scanning electron microscopy. The chemical analysis of the initial powders and sintered samples were measured by scanning electron microscopy equipped with energy dispersive spectroscope (EDS-SEM, JEOL IT 300 L V, Japan). The boron content of powders was confirmed by inductively coupled plasma/optical emission spectro-scopy (ICP/OES) using an Optima 8300 optical emission spectrometer (Perkin Elmer, USA). The carbon content of powders was determined by combustion elemental analysis (Carbon analyzer, EMIA-321 V, Horiba, Japan) and the oxygen, nitrogen and hydrogen contents of powders were measured using an EMGA-830 analyzer (Horiba, Japan). The thermal diffusivity of sintered samples was determined using a laser flash analyser (Linseis LFA 1000, Germany). Thin gold layer was de-posited on the surface of samples to spread the heat impulses homo-geneously on the surface of sample. Additionally, thin graphite layer was sprayed onto both sides of the samples before measurements to hinder any reflections of the laser beam or the sensitivity of IR sensor on the back side of sample. The measurements were carried out from room temperature up to 500 °C (with a step of 100 °C) in vacuum. At least three measurements were done at each temperature and the data were averaged. The thermal conductivities (λ) of samples were calculated

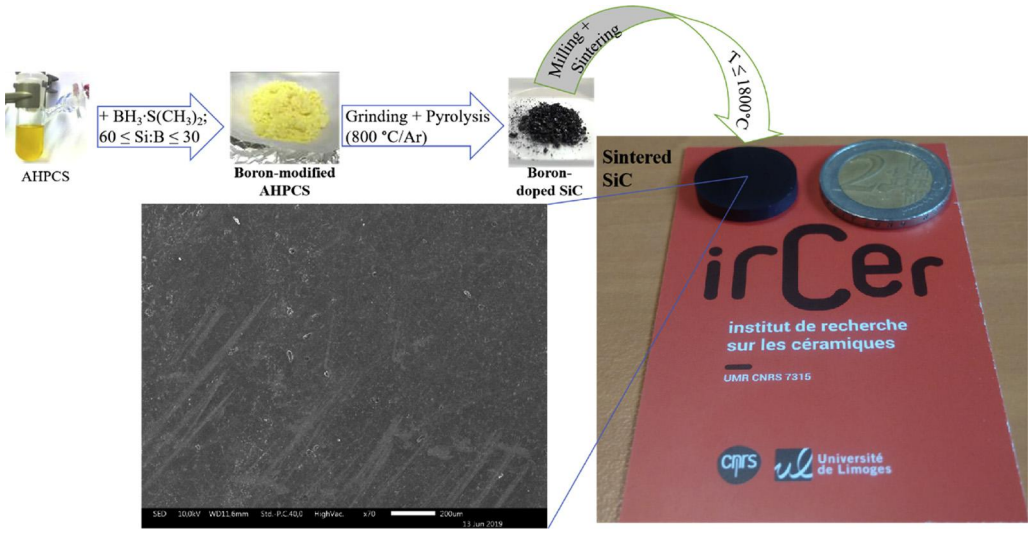


Fig. 1. Overall synthetic path employed to generate sintered SiC by pyrolysis of boron-modified AHPCS followed by rapid hot pressing of derived boron-doped SiC powders. High magnification SEM image of the SiBC30_18 sample as inset.

according the equation: $\lambda = \alpha \rho C_p$, where (α) is the thermal diffusivity (ρ) the density and C_p the heat capacity of samples. The heat capacity of silicon carbide 0.675 J/g K [44,45] was used for all samples, although some of the samples contained a small portion of carbon and silica. The electrical resistivity measurements were carried out at room tempera-ture using a standard four-point van der Pauw method [46]. The sur-faces of the specimens were polished to a mirror finish (1 μm) before the measurements. The bulk and apparent density values as well as open porosity of sintered samples were determined using the Archi-medes method in ethanol. Elastic properties were determined by an ultrasonic pulse echography technique based on the infinite medium mode using emitting/receiving contact transducers operating at a fre-quency of 10 MHz [47]. Longitudinal and transversal velocities were measured thanks to the wave propagation times of the waves in the thickness of disk-shaped samples. Previous apparent density in addition to these two velocity values is also required to estimate the Young's modulus. The Vickers hardness (HV) was measured by hardness tester LECO LV 100 (FutureTech Corp, USA) using an indentation load of 9.81 N.

3. Results and discussion

3.1. Preparation and characterization of amorphous powders

The SiBC60 and SiBC30 samples were produced by pyrolysis at 800 °C under argon of AHPCSB60 and AHPCSB30 samples, respectively. SiBC60 and SiBC30 samples were obtained in ca. 89.4 % and 91 % yields [43]. The empirical formula of the SiBC30 sample ($Si_{1.0}B_{0.03}C_{1.7}H_{0.8}O_{0.1}$) shows that the Si:B atomic ratio is almost un-changed compared to the polymer ($Si_{1.0}B_{0.034}C_{1.6}H_{4.7}$). This confirms that the composition of the powders can be controlled in the early stage of the process, i.e., at the atomic level in the polymer. As expected, powders show an excess of carbon as indicated by the Si:C atomic ratio and still contain residual hydrogen (linked to Si and C) according to the fact that the thermal decomposition of polymers is not fully achieved at 800 °C as shown through TG measurements performed under argon [43]. As an illustration, the hydrogen content in powders derived from AHPCSB30 changes from 1.50 wt.% after pyrolysis at 800 °C to 0.73 wt.

% after pyrolysis at 1000 °C and 0 wt.% after pyrolysis at 1500 °C. The as-obtained SiBC60 and SiBC30 samples are X-ray amorphous and contain free carbon which is reflected in the chemical formula and confirmed by Raman spectroscopy showing the disorder-induced D band and graphite-like G bands of free carbon (see Fig. 1SI in ESI).

3.2. Sintering of amorphous powders

Four samples labelled as SiBC60_17, SiBC60_18, SiBC30_17, SiBC30_18 have been prepared by sintering under argon at 1750 °C and 1800 °C. A typical example of sintered sample (SiBC30_18) obtained by RHP at 1800 °C is presented in Fig. 1. The microstructure and elemental composition of sintered samples at 1750 °C and 1800 °C for 15 min in Ar atmosphere was investigated on polished surfaces by SEM-EDS, the results are shown in Fig. 2 and Tables 1 and 2.

The elemental analyses of the samples provided in Table 1 show that the Si:B atomic ratio (from the calculated chemical formula) decreases from SiBC60_17 and SiBC60_18 samples to SiBC30_17 and SiBC30_18 samples in good agreement with the evolution of the Si:B atomic ratio fixed at the polymer level. The C content, which fits with the values found in the raw powders, suggests an excess of carbon in the sintered samples as identified in SiBC60 and SiBC30 samples. This is confirmed in Table 2 through the calculation of the phase content in each sintered sample. As expected, samples consist of SiC as a major phase and free carbon. A small content of silica is present in the majority of samples. However, the reason of the increased silica content in the samples sintered at 1800 °C, i.e., SiBC60_18 and SiBC30_18 is not known.

Fig. 2 shows that all samples have a structure with a clear grain cohesion and with relatively low residual porosity. However, the grain boundaries are not well visible in these SEM micrographs, as we have not used an oxide sintering additives for the densification of samples.

SEM images particularly show that the SiBC30_17 and SiBC30_18 samples display a relatively low level of porosity in contrast to the SiBC60_18 sample with a certain portion of large pores. Thus, the densities of former samples give a hint that we have reached the op-timal RHP conditions with the samples displaying the highest boron content (i.e., SiBC30_17 and SiBC30_18) to form nearly dense additive-free SiC ceramics. The densities of sintered samples are summarized in Table 3. The theoretical densities were calculated using the rule of mixture based on the phase composition (Table 2) of sintered samples and density values of β-SiC (3.21 g/cm^3), C (2.27 g/cm^3), B (2.37 g/cm^3) and SiO_2 (2.65 g/cm^3). The measured density values correspond with the SEM observations of porosity.

Samples with the lower boron content, i.e. SiBC60_18 and SiBC60_17 have significantly higher porosity compared to the samples with higher boron content, i.e., SiBC30_18 and SiBC30_17 samples. Sample SiBC60_18 displays the highest level of porosity, in good agreement with SEM images. Thus, the density/porosity values re-ported in Table 3 reflect the interest of both the introduction of boron at

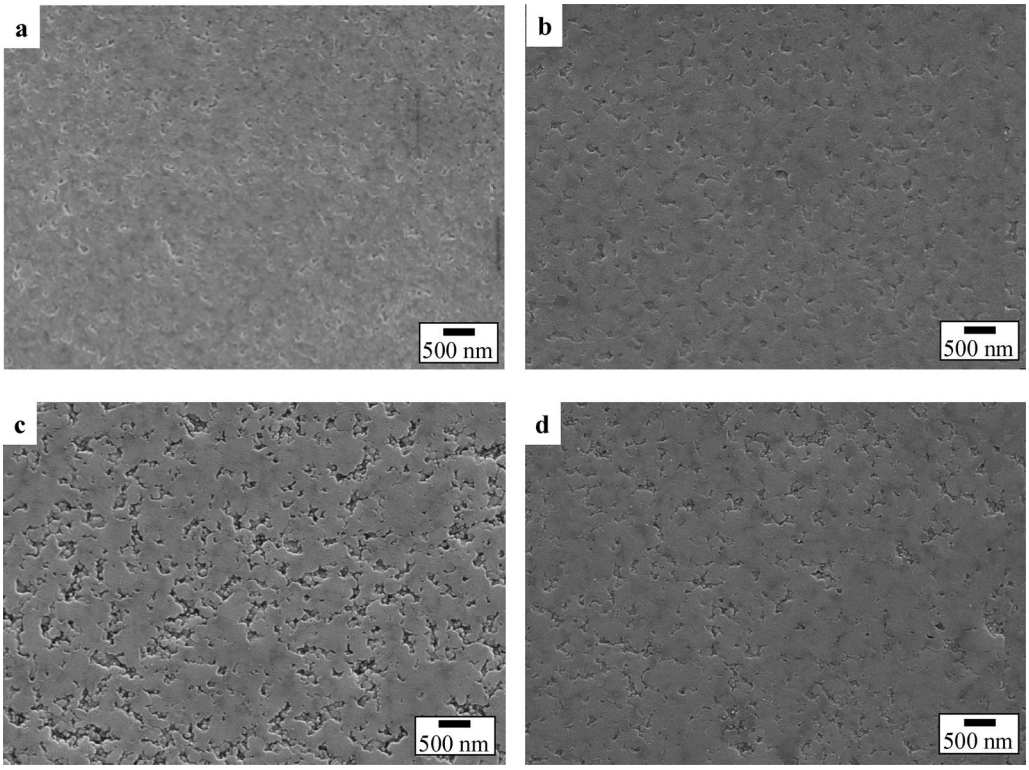


Fig. 2. SEM images of the sintered samples: SiBC60_17 (a), SiBC30_17 (b), SiBC60_18 (c) and SiBC30_18 (d).

Table 1
Elemental composition of sintered samples measured by Energy-Dispersive X-ray Spectroscopy (EDS). Empirical formulas are referenced to $Si_{1.0}$ and nor-malized to 100 wt.%.

Samples	Si (wt.%)	B (wt.%)	C (wt.%)	O (wt.%)	Chemical formula
SiBC60_17	57	3.2	38.9	0.9	$Si_{1.0}B_{0.1}C_{1.6}O_{0.03}$
SiBC60_18	58.8	3.1	36.4	1.7	$Si_{1.0}B_{0.1}C_{1.5}O_{0.05}$
SiBC30_17	56.1	4.1	38.7	1.1	$Si_{1.0}B_{0.2}C_{1.6}O_{0.03}$
SiBC30_18	54.2	4.0	38.2	3.6	$Si_{1.0}B_{0.2}C_{1.6}O_{0.1}$

Table 2
Calculated phase content in sintered samples based on elemental composition.

Samples	SiC (wt.%)	C (wt.%)	B (wt.%)	SiO_2 (wt.%)
SiBC60_17	80.9	15.1	2.2	1.8
SiBC60_18	82.2	13.3	2.3	3.2
SiBC30_17	79.1	14.8	4.3	1.8
SiBC30_18	74.6	15.3	4.2	5.9

Table 3
Apparent (ρ_a), bulk (ρ_b) and theoretical (ρ_{th}) densities, opened (P_o) and closed (P_c) porosities of samples.

Samples	ρ_a (g/cm^3)	ρ_b (g/cm^3)	ρ_{th} (g/cm^3)	P_o (%)	P_c (%)
SiBC60_17	2.66	2.93	3.04	9.2	3.6
SiBC60_18	2.51	2.98	3.08	15.8	3.3
SiBC30_17	2.97	3.03	3.03	2	0
SiBC30_18	2.93	2.94	3.00	0.3	2.0

molecular scale and the control of the Si:B atomic ratio in the pre-ceramic polymer. A polymer with an adjusted boron content, i.e. 0.7 wt. % of boron and Si:B atomic ratio of 30, can be synthesized by the pyrolysis of AHPCSB30 at 800 °C under argon into boron-doped SiC powders with a chemical composition of $Si_{1.0}B_{0.03}C_{1.7}H_{0.8}O_{0.1}$ that demonstrate sinterability by RHP at a temperature as low as 1750 °C to form nearly dense SiC-based ceramics.

3.3. Phase identification in sintered objects

The crystalline phase composition of samples determined by XRD analysis are shown in Fig. 3, the Raman spectra on Fig. 4.

XRD analyses show that the low temperature β-SiC (3C) polytype is the major phase in all samples. The presence of hexagonal polytypes of α-SiC (6H-SiC) is identified by additional peaks emerging at 34.08° for plane (101) and at 38.3° for plane (103), although with weaker in-tensities for SiBC30_17 and SiBC30_18 samples.

All patterns show a diffraction in the range of 26.12° - 26.35° which corresponds to the (002) reflection of graphite. Its intensity increases in the XRD patterns of SiBC30_17 and SiBC30_18 samples. No additional phases have been detected in all XRD patterns. A semi-quantitative estimation of the extent of crystallization in sintered samples was achieved by calculating the integrated intensity of the Gaussian–Lorentzian curve fitting of the diffraction (002) from free carbon and (220) from β-SiC lines. These peaks were chosen based on the sufficient freedom from peak overlap. Peak positions have been measured and crystallite sizes have been calculated from the FWHM of the above diffraction lines using the Scherrer formula (Table 4). The lattice parameter of cubic SiC has been also calculated.

By comparing the corresponding crystallite size values of the re-spective samples in Table 4, it can be seen that SiC crystal growth is more pronounced in samples with higher boron content, i.e. in samples SiBC30_17 and SiBC30_18, respectively. Thus, the gradual incorpora-tion of boron in the early stage of the process from AHPCS60 to AHPCS30 enhances the tendency of the crystallization of β-SiC in the sintered samples derived from SiBC60_X to SiBC30_X (X being 17 or 18). This was experimentally demonstrated on other PDCs systems in-cluding silicon boron oxycarbide (SiBeOeC) glasses [48] and silicon

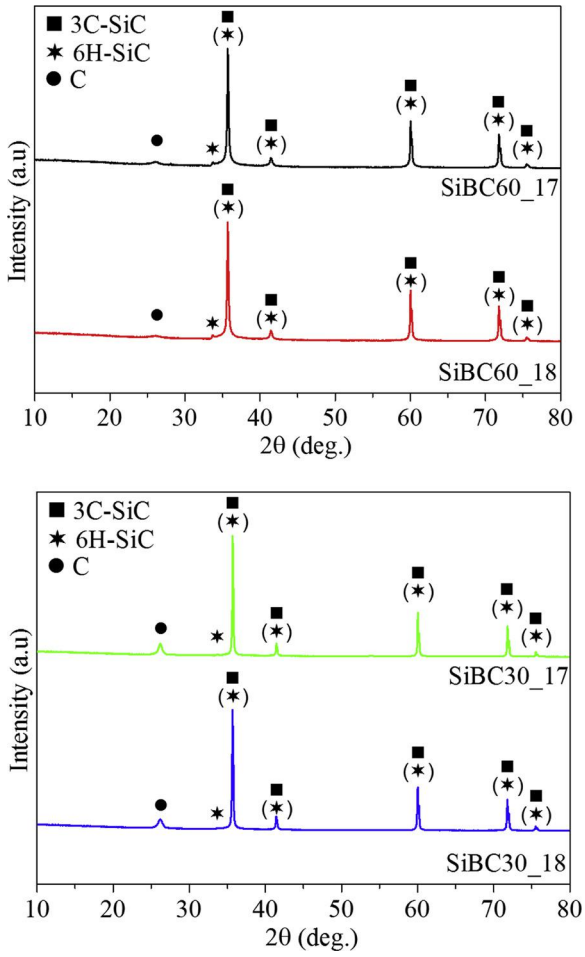


Fig. 3. XRD patterns of the sintered samples.

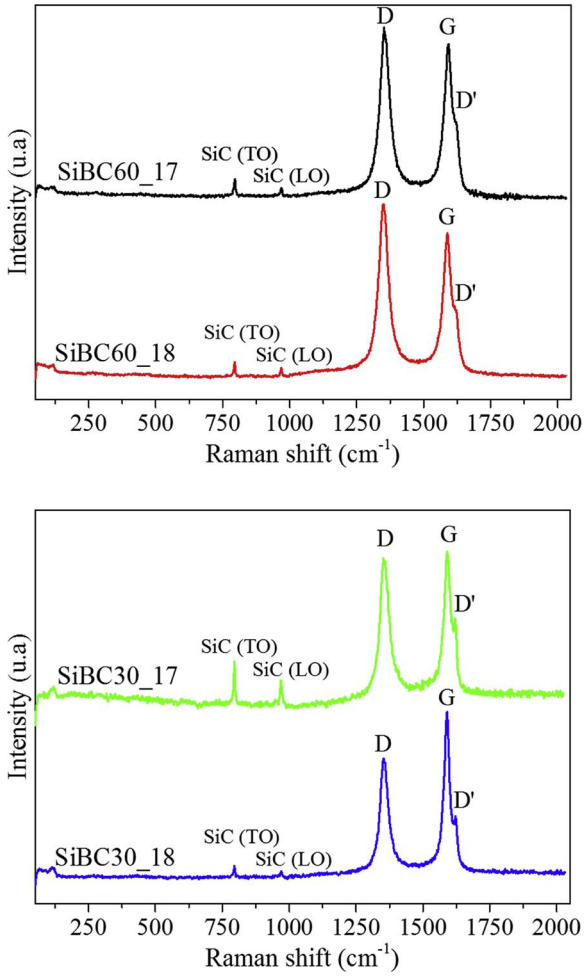


Fig. 4. Raman spectra of the sintered samples.

boron carbonitride (SieBeCeN) ceramics [49,50]. In particular, Ta-vakoli et al. [49] showed in the thermodynamic modeling that boron increased the crystallization of β-SiC from the amorphous SieCeN domains. At the same boron content, the temperature of sintering promotes the crystallization of SiC, as expected. Kaur et al. [42] de-monstrated that the lattice parameter of β-SiC is not affected by the boron content in the samples and it slightly decreases with the tem-perature of sintering. The calculated values of lattice parameters were lower than those found for the boron-free SiC powders prepared at 1900 °C (not sintered under pressure) [42]. Considering that an increase of the lattice parameter of β-SiC is due to boron incorporation into the β-SiC phase [51] whereas its reduction is associated with the formation of a SiC/C solid solution [52], this confirms in agreement with the results of Kaur et al. for a similar B-doped SiC system [42] that no boron is incorporated into the β-SiC lattice in our sintered samples.

Table 4

Full width at half maximum (FWHM), 2θ diffraction angle, crystallite size (D_{SiC}) for SiC, lattice parameter (a) for SiC and crystallite thickness (L_c) for free carbon obtained from XRD data of (220) β-SiC and (002) of carbon.

Samples	β-SiC (220)				Carbon (002)		
	FWHM (°)	2θ (°)	D_{SiC} (nm)	a (nm)	FWHM (°)	2θ (°)	L_c (nm)
SiBC60_17	0.152	60.04	60.4	0.436	1.16	26.12	7.0
SiBC60_18	0.142	60.14	64.6	0.435	1.75	26.16	4.7
SiBC30_17	0.124	60.01	74.0	0.436	0.62	26.21	13.1
SiBC30_18	0.115	60.11	79.8	0.435	0.70	26.35	11.7

The gradual shift of the (002) diffraction peak of graphite toward the theoretical position (26.5°, Table 4 and Fig. 2SI in ESI) indicates the formation of more compact and ordered carbon nanodomains in the SiBC30_17 and SiBC30_18 samples, i.e. enhanced by the increased boron content. As a consequence, the d_{002} spacing decreases from 0.341 nm (SiBC60-17) to 0.338 nm (SiBC30_18). Furthermore, the carbon crystallite size in the c-axis (L_c, crystallite thickness for graphite or stacking for all types of carbon phases, Table 4) increases with the in-creased boron content (the FWHM of the (002) peak decreases, see Fig. 2SI in ESI). This is, again, consistent with the results reported by Kaur et al. [42] and in good agreement with the results reporting that boron can accelerate graphitization of the materials [53,54]. Indeed, boron atoms can diffuse into the hexagonal basal planes of graphite and substitute carbon atoms to an extend of less than 2.5–3.0 at.% in order to rearrange the framework structure of carbon atoms [53]. This pro-motes the growth and orientation of crystallite and tends to decrease the total number of accessible active surface sites for oxygen [54]. This phenomenon is used to improve the resistance of carbon/carbon com-posites toward oxidation [54]. Thus, in the present work, the decrease of d_{002} is most probably due to both the crystallinity improvement re-sulting from the addition of boron and to the lowering in electron density due to the B substitution. However, this does not induce the formation of boron carbide-based phases based on the XRD analysis of prepared samples. More detailed TEM analysis are carried out to in-vestigate the formation of boron carbide-based clusters, nanocrystals, and the results will be published separately. In contrast, the crystallite thickness L_c decreases with the increase of the sintering temperature at a constant boron content (Table 4). For a better understanding of the structure and phase evolutions during RHP sintering, the samples have

been investigated by Raman spectroscopy (Fig. 4).

Compared to raw powders, i.e. SiBC60 and SiBC30 samples (see Fig. 1SI in ESI), the Raman spectra of sintered samples exhibit two bands centered at 795 cm^{-1} and 969 cm^{-1} assigned to the transversal-optical (TO) and longitudinal-optical (LO) modes of β-SiC, respectively [55]. This confirms the nucleation of β-SiC in sintered samples from the amorphous SiC phase present in SiBC60 and SiBC30 powders. Raman spectroscopy is one of the most sensitive techniques to characterize the disorder in sp^2 carbon materials. The spectra of sintered samples exhibit very distinct and narrow bands of the defect-induced D (originates from the breathing mode A_{1g} of the sp^2 rings) and graphitic G bands (arises from the stretching mode E_{2g} of the sp^2 CeC bonds) at 1355 cm^{-1} and 1590 cm^{-1}, respectively. The D band is a defect induced double resonance peak that occurs due to inelastic scattering by a phonon and elastic scattering by a defect [56]. Thus, the D-mode is caused by dis-ordered structure in sp^2-hybridized carbon systems. Hence, more dis-ordered samples should exhibit higher D band intensities. Considering that the G band is characteristic of highly ordered carbon species, the ratio of integrated intensity of the D band to that of the G band (I(D)/I (G)) is a good indicator of sample crystallinity, in other words it characterizes the degree of disorder. In order to follow the structural changes in the sintered samples, a multiple peak Gaussian–Lorentzian curve fitting procedure was performed in order to extract information such as the I(D)/I(G) ratio. The data are plotted in Fig. 5. The evolution of the D and G peak widths (FWHM) are also reported.

Whereas the D and G peak positions are nearly the same in all samples, the increase in the intensity of the G band and the concomitant decrease of the D band (Fig. 4), i.e. the decrease of the I(D)/I(G) ratio from SiBC60_17 to SiBC30_18 (Fig. 5) tends to confirm the formation of more ordered carbon nanodomains in samples with the highest boron content (SiBC30_17 and SiBC30_18 samples, Fig. 5). In addition, Fig. 4 shows the clear appearance of an additional D' band located at 1620 cm^{-1} as a shoulder of the G-band in all samples, which is more visible in samples with the highest boron content (SiBC30_17 and SiBC30_18, Fig. 4). The visibility of D' band is pronounced by the continuous de-crease of the G peak width from SiBC60_17 to SiBC30_18 samples, i.e. FWHM (Fig. 5). Free disordered carbon in PDCs usually contribute to the signals of the D and G bands [57,58], but the D' band does not appear because of its overlapping by the enlarged G band peak. This peak is indicative of sp^2 bonded carbon that represents surface defect modes (distortion in graphite). The D and D' bands can give rise to overtones and combination modes, thereby resulting in additional symmetry-breaking modes in the Raman spectra [59]. The most common reasons for symmetry breaking are the presence of vacancies, interstitial atoms, and substitutional atoms. Thus, the increase of the I (D)/I(G) ratio from 1.1 for SiBC60_17 to 1.2 for SiBC60_18 (Fig. 5), indicates the increase of defects in the later sample whereas its decrease for the SiBC30_X (X = 17 and 18) samples is due to the increase of the

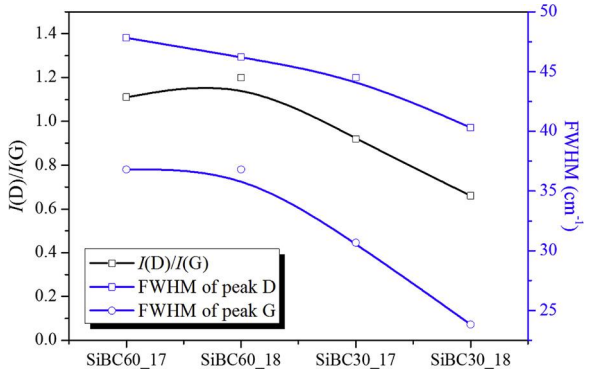


Fig. 5. Raman analysis of sintered samples: variation of FWHM of D and G bands and the intensity ratio I(D)/I(G) with the sintering temperature and the boron content.

Table 5
Mechanical properties of sintered samples (HV – Vickers hardness, E - elastic modulus).

Samples	HV (GPa)	E (GPa)
SiBC60_17	16.6 ± 1.2	193 ± 5
SiBC60_18	9.6 ± 0.5	137 ± 3
SiBC30_17	17.3 ± 1.9	239 ± 6
SiBC30_18	11.0 ± 0.6	179 ± 4

ordering degree of the carbon phase [60]. Furthermore, the continuous decrease of the FWHM of the D and G peaks is probably due to the site-to-site variation in the number of next nearest neighbours (i.e. sp^2 C atoms have B neighbours). It is important to mention that the sintering temperature (1750 °C vs 1800 °C) has an effect on the structural or-ganization of free carbon only at a certain boron content (4 wt.%) contained in sintered samples.

3.4. Mechanical and physical properties of sintered samples

The measured Vickers hardness and Young's modulus of sintered samples are summarized in Table 5 and reflects the effect of the above-mentioned structural changes in the prepared materials.

The isotropy of samples in elastic properties has been verified with ultrasonic pulse echography method. Indeed, due to uniaxial hot-pressing of samples a preferred orientation of the grains could be pro-moted perpendicular to the axial loading. In general, the measured mechanical properties are lower compared to those for dense SiC (i.e. Young's modulus of 460 GPa and Vickers hardness of 27 GPa [61]). The obtained lower mechanical properties are related to the presence of free carbon and in some cases also silica in the final materials. The hardness of the turbostratic carbon observed in the samples is indeed as low as 0.9 GPa [62]. However, the hardness values obtained for samples sin-tered at 1750 °C (HV = 16.6 ± 1.2 GPa (SiBC60_17) and HV = 17.3 ± 1.9 GPa (SiBC30_17)) are significantly higher than those re-ported for SiC materials prepared by SPS of AHPCS-derived SiC (without introduction of boron in AHPCS) at similar temperatures: HV = 6.0 ± 0.3 GPa after SPS at 1700 °C and HV = 9.0 ± 0.3 GPa after SPS at 1800 °C [35]. This highlights the interest of modifying AHPCS with borane dimethylsulfide to add boron at molecular scale and im-prove the sinterability of AHPCS-derived SiC powders during sintering process. Considering a same boron content, the highest mechanical properties were obtained for samples sintered at 1750 °C, i.e., SiBC60_17 (HV = 16.6 ± 1.2 GPa; E = 193 ± 5 GPa) and SiBC30_17 (HV = 17.3 ± 1.9 GPa; E = 239 ± 6 GPa) samples. The mechanical properties of samples sintered at 1800 °C drop by 30 %. The hardness being usually reported to increase with decreasing grain size for non-oxide ceramics in analogy to the findings of Hall and Petch for metals [63–65]. The Hall-Petch effect is valid also for the samples sintered at 1750 °C in which the β-SiC crystallite sizes are the smallest, 60.40 nm and 60.14 nm (at a constant boron content, see Table 4). However, the larger crystallite size of samples sintered at 1800 °C is most probably not the key reason of the significant decrease of the mechanical prop-erties of SiBC60_18 (HV = 9.6 ± 0.5 GPa; E = 137 GPa ± 3.4) and SiBC30_18 (HV = 11.0 ± 0.6 GPa; E = 179 GPa ± 4) samples. Another factor influencing the hardness is the phase composition. In samples sintered at 1800 °C the SiC content is lower, while the content of softer phases as carbon and SiO_2 is higher compared to samples sintered at 1750 °C (Table 2), therefore their hardness is lower. The low Vickers hardness of sample SiBC60_18 (HV = 9.6 GPa) is related also to the high level of porosity (15.8 %, Table 3), as the hardness of sample SiBC60_17 with 9.2 % porosity increased significantly (HV = 16.6 GPa). The measured values of Young's modulus follow the trend of the Vickers hardness. The decrease of the elastic modulus of sample SiBC30_18 can be attributed to the lowest SiC content (and the highest

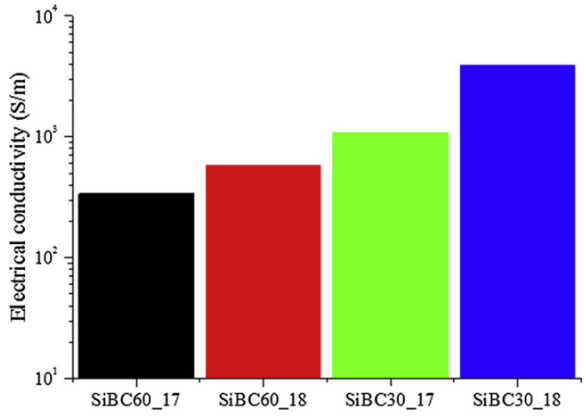


Fig. 6. Electrical conductivity measurements of sintered samples.

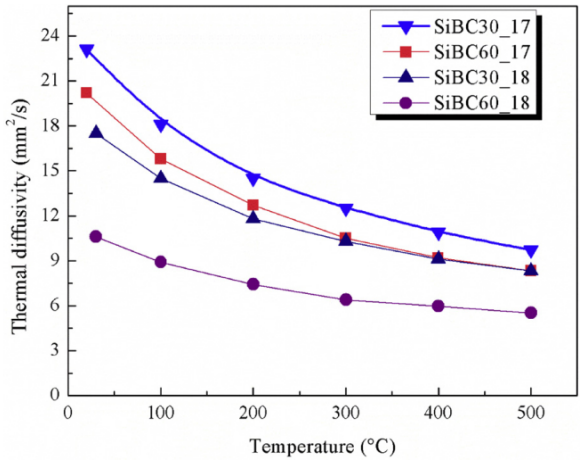


Fig. 7. Variation of the thermal diffusivity of sintered samples with tempera-ture.

silica content), higher porosity and probably also to the direct inter-action of carbon nanodomains. The interaction of carbon phases is supported by the increased electrical conductivity of the sintered samples.

The results of preliminary investigations of the electrical con-ductivity of samples measured in the direction perpendicular to the RHP axis are shown in Fig. 6 and summarized in Table 6. Here, the purpose of this study is not to provide a detailed study of the electrical properties but a picture of the effect of the structure/composition on the electrical resistivity and conductivity.

Interestingly, Fig. 6 depicts an approximately linear dependence of $\log_{10}$ σ vs. boron content and sintering temperature, both affecting crystal growth, carbon content and carbon nanodomain organization. The carbon contents measured in all sintered samples and the expected high aspect ratio of the segregated carbon in those materials probably indicate that both compositions are above the percolation threshold concerning the electrical conductivity. However, Fig. 5 demonstrates that the ordering degree of the carbon phase increases with the increase of both the boron content and the sintering temperature. The electrical resistivity (κ measured at 10 mA, continuously decreases from 0.296 Ω cm for SiBC60_17 to 0.026 Ω cm for SiBC30_18 (Table 6). The ob-served trend is strongly affected by the increase of the ordering degree of the carbon phase in the sintered samples, as the I(D)/I(G) in the Raman spectra remarkably decreased from 1.11 to 0.68 (Fig. 5). Ac-cordingly, the electrical conductivity continuously increases from the SiBC60_17 sample to the SiBC30_18 sample (Fig. 6). The measured electrical conductivity of the SiBC30_18 sample is significantly higher (3906 S/m) than that reported for SiC and is comparable to those measured for graphene/SiC composites [66].

The thermal diffusivities of sintered samples (measured in direction parallel to the RHP axis) in the temperature range of 20 °C – 500 °C are shown in Fig. 7. It is known that the thermal conductivity in covalently bonded ceramic materials is controlled by phonon transport, therefore it strongly depends on the microstructure (impurities, microcracks, porosity and the grain boundary phases). Boron is soluble in SiC [67], thus B atoms as well as other dopants play a role in scattering of pho-nons, and decreasing the heat transfer.

The variation of the thermal diffusivity of each sample with the test temperature is similar. It decreases with increasing test temperature which is related to the increased phonon scattering due to the higher degree of anharmonicity [68]. The SiBC30_17 sample displays the highest thermal diffusivities due to the relatively high content of heat-conductive SiC and free carbon phases whereas the silica content is very low. Furthermore, the total porosity measured in this sample is the lowest. An increase of the porosity in sintered samples inherently in-volves a decrease of their thermal diffusivity; this is particularly ob-vious in the most porous SiBC60_18 sample that displays the lowest thermal diffusivity. The situation is a bit more complex with the SiBC30_18 sample which displays a low level of porosity. The main difference between SiBC30_17 and SiBC30_18 samples is the relatively high silica content in the latter, which can significantly decrease the thermal diffusivity of SiC-based ceramics.

In line with the changes observed in the variation of the thermal diffusivity, the thermal conductivity values (Table 6) decreases from 45.1 W/m K (SiBC30_17) to 17.7 W/m K (SiBC60_18) with the increase of the total porosity of sintered samples. In addition to the effect of porosity also the negative effect of higher oxygen content in SiC sam-ples sintered at 1800 °C cannot be excluded, as it can contribute (re-markably) to the decrease of the thermal conductivity of samples.

Table 6
Electrical resistivity (κ at 10 mA, thermal diffusivity (α) and thermal con-ductivity (λ) at 20 °C of sintered samples.

Samples	κ (Ω cm)	α (mm^2/s)	λ (W/m K)
SiBC60_17	0.296	20.2	35.3
SiBC60_18	0.172	10.6	17.7
SiBC30_17	0.093	23.1	45.1
SiBC30_18	0.026	17.5	33.8

4. Conclusion

Additive-free SiC ceramics have been prepared by combining the PDCs route to elaborate amorphous polymer-derived Si-B-C powders consisting of Si linked to C and homogeneously distributed sintering aids (B and C) on atomic level with field assisted sintering technology (rapid hot-pressing, RHP) to densify raw powders in the temperature range of 1750−1800 °C and under a load of 50 MPa. The structural, mechanical and physical properties including electrical and thermal conductivities of sintered samples have been experimentally de-termined. In the processing of samples, allylhydridopolycarbosilane (AHPCS) was used as a SiC precursor to introduce boron at molecular scale in order to form boron-modified AHPCS polymers and produce the derived boron-doped SiC powders with an adjusted boron content after pyrolysis at 800 °C. Si-B-C powders were sintered at at relatively tem-perature (1750 °C) without ex-situ sintering additives. The level of porosity of sintered samples significantly decreased with the increase of the boron content in samples. Boron is preferentially incorporated into the carbon phase rather than in the β-SiC phase and affects the carbon nanodomain ordering within the sintered samples. The effect of these variations is reflected in the mechanical and physical properties of the prepared materials. The SiC ceramics sintered at temperatures as low as 1750 °C exhibit a Vickers hardness and an elastic modulus as high as

17.3 ± 1.9 GPa and 239 ± 6 GPa, respectively. The mechanical prop-erties are affected by the phase composition (determined by the Si:B atomic ratio and oxygen content), the crystal growth (β-SiC and sp^2-carbon) and the volume fraction of porosity in the materials. Accordingly, the electrical conductivities varied from 340 S/m to 3900 S/m and the thermal conductivities changed from 17.7 W/m K to 45.1 W/m K, depending on the density and phase composition of samples. The results showed that polycarbosilane with an adjusted boron content of 0.7 wt.% leads to boron-doped SiC powders with a tailored chemical composition that demonstrate sinterability by RHP at a temperature as low as 1750 °C and 1800 °C to form nearly dense SiC-based ceramics with adjusted hardness, Young's modulus, electrical and thermal con-ductivities. The combination of the PDCs route for Si-B-C powder pre-paration and RHP sintering method for the densification of SiC samples appears to be a promising method for the preparation of SiC ceramics with tunable mechanical and thermo-physical properties.

References

[1] L. Stobierski, A. Gubernat, Sintering of silicon carbide I. Effect of carbon, Ceram. Int. 29 (2003) 287–292, https://doi.org/10.1016/S0272-8842(02)00117-7.

[2] L. Stobierski, A. Gubernat, Sintering of silicon carbide II. Effect of boron, Ceram. Int. 29 (2003) 355–361, https://doi.org/10.1016/S0272-8842(02)00144-X.

[3] M. Khodaei, O. Yaghobizadeh, S.H.N. Alhosseini, S. Esmaeeli, S.R. Mousavi, The effect of oxide, carbide, nitride and boride additives on properties of pressureless sintered SiC: a review, J. Eur. Ceram. Soc. 39 (2019) 2215–2231, https://doi.org/10.1016/j.jeurceramsoc.2019.02.042.

[4] K. Raju, D.-H. Yoon, Sintering additives for SiC based on the reactivity: a review, Ceram. Int. 42 (2016) 17647–17962, https://doi.org/10.1016/j.ceramint.2016.09. 022.

[5] M. Birot, J.-P. Pillot, J. Dunogues, Comprehensive chemistry of polycarbosilanes, polysilazanes, and polycarbosilazanes as precursors of ceramics, Chem. Rev. 95 (1995) 1443–1477, https://doi.org/10.1021/cr00037a014.

[6] J. Bill, F. Aldinger, Precursor-derived covalent ceramics, Adv. Mater. 7 (1995) 775–787, https://doi.org/10.1002/9783527613823.ch4.

[7] P. Greil, Polymer derived engineering ceramics, Adv. Eng. Mater. 2 (2000) 339–348, https://doi.org/10.1002/1527-2648(200006)2:6<339::AID-ADEM339>3.0.CO;2-K.

[8] P. Colombo, G. Mera, R. Riedel, G.D. Soraru, Polymer-derived ceramics: 40 years of research and innovation in advanced ceramics, J. Am. Ceram. Soc. 93 (2010) 1805–1837, https://doi.org/10.1111/j.1551-2916.2010.03876.x.

[9] E. Ionescu, H.-J. Kleebe, R. Riedel, Silicon-containing polymer-derived ceramic nanocomposites (PDC-NCs): preparative approaches and properties, Chem. Soc. Rev. 41 (2012) 5032–5052, https://doi.org/10.1039/C2CS15319J.

[10] M. Zaheer, T. Schmalz, G. Motz, R. Kempe, Polymer derived non-oxide ceramics modified with late transition metals, Chem. Soc. Rev. 41 (2012) 5102–5116, https://doi.org/10.1039/c2cs15326b.

[11] S. Bernard, P. Miele, Polymer-derived boron nitride: a review on the chemistry, shaping and ceramic conversion of borazine derivatives, Materials 7 (2014) 7436–7459, https://doi.org/10.3390/ma7117436.

[12] G. Mera, M. Gallei, S. Bernard, E. Ionescu, Ceramic nanocomposites from tailor-made preceramic polymers, Nanomaterials 5 (2015) 468–540, https://doi.org/10.3390/nano5020468.

[13] C. Stabler, E. Ionescu, M. Graczyk-Zajac, I. Gonzalo-Juan, R. Riedel, Silicon oxy-carbide glasses and glass-ceramics: "All-Rounder" materials for advanced structural and functional applications, J. Am. Ceram. Soc. 101 (2018) 4817–4856, https://doi.org/10.1111/jace.15932.

[14] A. Viard, D. Fonblanc, D. Lopez-Ferber, M. Schmidt, A. Lale, C. Durif, M. Balestrat, F. Rossignol, M. Weinmann, R. Riedel, S. Bernard, Polymer derived Si-B-C-N ceramics: 30 years of research, Adv. Eng. Mater. 20 (2018) 1800360–1800371, https://doi.org/10.1002/adem.201800360.

[15] E. Ionescu, S. Bernard, R. Lucas, P. Kroll, S. Ushakov, A. Navrotsky, R. Riedel, Ultrahigh temperature ceramics (UHTCs) and related materials – syntheses from polymeric precursors and energetics, Adv. Eng. Mater. 21 (2019) 1900269–1900292, https://doi.org/10.1002/adem.201900269.

[16] A. Lale, M. Schmidt, M.D. Mallmann, A.V.A. Bezerra, E. Diz Acosta, R.A.F. Machado, U.B. Demirci, S. Bernard, Polymer-derived ceramics with en-gineered mesoporosity: from design to application in catalysis, Surf. Coat. Technol. 350 (2018) 569–586, https://doi.org/10.1016/j.surfcoat.2018.07.061.

[17] A. Viard, P. Miele, S. Bernard, Polymer-derived ceramics route toward SiCN and SiBCN fibers: from chemistry of polycarbosilazanes to the design and character-ization of ceramic fibers, J. Ceram. Soc. Jpn. 124 (2016) 967–980, https://doi.org/10.2109/jcersj2.16124.

[18] O. Flores, R.K. Bordia, D. Nestler, W. Krenkel, G. Motz, Ceramic fibers based on SiC and SiCN systems: current research, development, and commercial status, Adv. Eng. Mater. 16 (2014) 621–636, https://doi.org/10.1002/adem.201400069.

[19] G. Barroso, Q. Li, R.K. Bordia, G. Motz, Polymeric and ceramic silicon-based coat-ings – a review, J. Mater. Chem. A 7 (2019) 1936–1963, https://doi.org/10.1039/C8TA09054H.

[20] C. Vakifahmetoglu, D. Zeydanli, P. Colombo, Porous polymer derived ceramics, Mater. Sci. Eng. R 106 (2016) 1–30, https://doi.org/10.1016/j.mser.2016.05.001.

[21] A. Viard, D. Fonblanc, M. Schmidt, A. Lale, C. Salameh, A. Soleilhavoup, M. Wynn, P. Champagne, S. Cerneaux, F. Babonneau, G. Chollon, F. Rossignol, C. Gervais, S. Bernard, Molecular chemistry and engineering of boron-modified poly-organosilazanes as new processable and functional SiBCN precursors, Chem. Eur. J. 23 (2017) 9076, https://doi.org/10.1002/chem.201700623.

[22] D. Fonblanc, D. Lopez-Ferber, M. Wynn, A. Lale, A. Soleilhavoup, A. Leriche, Y. Iwamoto, F. Rossignol, C. Gervais, S. Bernard, Crosslinking chemistry of poly (vinylmethyl-co-methyl)silazanes toward low-temperature formable preceramic polymers as precursors of functional aluminium-modified Si-C-N ceramics, Dalton Trans. 47 (2018) 14580–14593, https://doi.org/10.1039/C8DT03076F.

[23] S. Kaur, R. Riedel, E. Ionescu, Pressureless fabrication of dense monolithic SiC ceramics from a polycarbosilane, J. Eur. Ceram. Soc. 34 (2014) 3571–3578, https://doi.org/10.1016/j.jeurceramsoc.2014.05.002.

[24] M.C. Bechelany, V. Proust, C. Gervais, R. Ghisleni, S. Bernard, P. Miele, In-situ controlled growth of titanium nitride in amorphous silicon nitride: a general route toward bulk non-oxide nitride nanocomposites with very high hardness, Adv. Mater. 26 (2014) 6548–6553, https://doi.org/10.1002/adma.201402356.

[25] M.C. Bechelany, V. Proust, A. Lale, P. Miele, S. Malo, C. Gervais, S. Bernard, Nanocomposites through chemistry of single-source precursors: Understanding the role of chemistry behind the design of monolith-type nanostructured titanium ni-tride/silicon nitride, Chem. Eur. J. 23 (2017) 832–845, https://doi.org/10.1002/ chem.201603661.

[26] R. Riedel, M. Seher, J. Mayer, D. Vinga Szabó, Polymer-derived Si based bulk ceramics. Part I. Preparation, processing and properties, J. Eur. Ceram. Soc. 15 (1995) 703–715, https://doi.org/10.1016/0955-2219(95)00041-R.

[27] W. Dressler, A. Greiner, M. Seher, R. Riedel, Fabrication of nanostructured ceramics by hybrid processing, Nanostruct. Mater. 6 (1995) 481–484, https://doi.org/10. 1016/0965-9773(95)00101-8.

[28] H.-J. Kleebe, H. Schmidt, W. Lehner, G. Ziegler, Organometallic precursors, an al-ternative route for the doping of silicon nitride powders, J. Eur. Ceram. Soc. 22 (2002) 955–961, https://doi.org/10.1016/S0955-2219(01)00397-1.

[29] T. Plachký, Z. Lenčéš, Ľ. Hric, P. Šajgalík, P. Baláž, R. Riedel, H.-J. Kleebe, Processing and mechanical properties of Si_3N_4 composites employing polymer-de-rived SiAlOC as sintering aid, J. Eur. Ceram. Soc. 30 (2010) 759–767, https://doi.org/10.1016/j.jeurceramsoc.2009.08.014.

[30] S. Ishihara, H. Gu, J. Bill, F. Aldinger, F. Wakai, Densification of precursor-derived Si-C-N ceramics by high-pressure hot isostatic pressing, J. Am. Ceram. Soc. 85 (2002) 1706–1712, https://doi.org/10.1111/j.1151-2916.2002.tb00339.x.

[31] M.J. Gasch, J. Wan, A.K. Mukherjee, Preparation of a Si_3N_4/SiC nanocomposite by high-pressure sintering of polymer precursor derived powders, Scripta Mater. 45 (2001) 1063–1068, https://doi.org/10.1016/S1359-6462(01)01140-X.

[32] O. Majoulet, M.C. Bechelany, F. Sandra, G. Bonnefont, G. Fantozzi, L. Joly-Pottuz, A. Malchere, S. Bernard, P. Miele, Silicon-boron-carbon-nitrogen monoliths with high, interconnected and hierarchical porosity, J. Mater. Chem. A 1 (2013) 10991–11000, https://doi.org/10.1039/C3TA12119D.

[33] M.C. Bechelany, C. Salameh, A. Viard, L. Guichaoua, F. Rossignol, T. Chartier, S. Bernard, P. Miele, Preparation of polymer-derived Si-B-C-N monoliths by spark plasma sintering technique, J. Eur. Ceram. Soc. 35 (2015) 1361–1374, https://doi.org/10.1016/j.jeurceramsoc.2014.11.021.

[34] J. Yuan, D. Li, K.E. Johanns, C. Fasel, K. Durst, H.-J. Kleebe, Z. Shen, R. Riedel, E. Ionescu, Preparation of dense SiHf(B)CN-based ceramic nanocomposites via rapid spark plasma sintering, J. Eur. Ceram. Soc. 37 (2017) 5157–5165, https://doi.org/10.1016/j.jeurceramsoc.2017.04.066.

[35] A. Rahman, A. Singh, S.P. Harimkar, R.P. Singh, Mechanical characterization of fine grained silicon carbide consolidated using polymer pyrolysis and spark plasma sintering, Ceram. Int. 40 (2014) 12081–12091, https://doi.org/10.1016/j.

ceramint.2014.04.048.
[36] F. Delobel, S. Lemonnier, E. Barraud, J. Cambedouzou, Influence of sintering temperature and pressure on the 3C-6H transition of silicon carbide, J. Eur. Ceram. Soc. 39 (2019) 150–156, https://doi.org/10.1016/j.jeurceramsoc.2018.09.010.
[37] C.K. Whitmarsh, L.V. Interrante, Carbosilane polymer precursors to silicon carbide ceramics, U.S. Patent No. 5,153,295, October 6: 1992.
[38] Starfire Systems, Inc., 877 25th St., Watervliet, NY, 12189.
[39] F. Sandra, A. Ballestero, V.L. NGuyen, M.N. Tsampas, P. Vernoux, C. Balan, Y. Iwamoto, U.B. Demirci, P. Miele, S. Bernard, Silicon carbide-based membranes with high filtration efficiency, durability and catalytic activity for CO/HC oxidation and soot combustion, J. Membr. Sci. 501 (2016) 79–92, https://doi.org/10.1016/j.memsci.2015.12.015.
[40] V. Proust, M.C. Bechelany, R. Ghisleni, M.F. Beaufort, P. Miele, S. Bernard, Polymer-derived Si-C-Ti systems: from titanium nanoparticle-filled polycarbosilanes to dense monolithic multi-phase components with high hardness, J. Eur. Ceram. Soc. 36 (2016) 3671–3679, https://doi.org/10.1016/j.jeurceramsoc.2016.04.023.
[41] A.R. Puerta, E.E. Remsen, M.G. Bradley, S. Sherwood, L.G. Sneddon, Synthesis and ceramic conversion reactions of 9-BBN-modified allylhydridopolycarbosilane: a new single-source precursor to boron-modified silicon carbide, Chem. Mater. 15 (2003) 478–485, https://doi.org/10.1021/cm020697i.
[42] S. Kaur, G. Mera, R. Riedel, E. Ionescu, Effect of boron incorporation on the phase composition and high-temperature behavior of polymer-derived silicon carbide, J. Eur. Ceram. Soc. 36 (2016) 967–977, https://doi.org/10.1016/j.jeurceramsoc.2015.11.037.
[43] M. Schmidt, C. Durif, E. Diz Acosta, C. Salameh, H. Plaisantin, P. Miele, R. Backov, R. Machado, C. Gervais, J.G. Alauzun, G. Chollon, S. Bernard, Molecular-level processing of Si-(B)-C materials with tailored nano/microstructures, Chem. Eur. J. 23 (2017) 17103–17117, https://doi.org/10.1002/chem.201703674.
[44] G.-D. Zhan, M. Mitomo, R.-J. Xie, A.K. Mukherjee, Thermal and electrical properties in plasma activation sintered silicon carbide with rare earth oxide additives, J. Am. Ceram. Soc. 84 (2001) 2448–2450, https://doi.org/10.1111/j.1151-2916.2001. tb01033.x.
[45] Y. Li, J. Yin, H. Wu, P. Lu, Y. Yan, X. Liu, Z. Huang, D. Jiang, High thermal conductivity in pressureless densified SiC ceramics with ultra-low contents of additives derived from novel boron–carbon sources, J. Eur. Ceram. Soc. 34 (2014) 2591–2595, https://doi.org/10.1016/j.jeurceramsoc.2014.02.024.
[46] L.J. Van der Pauw, A method of measuring specific resistivity and Hall effect of discs of arbitrary shape, Philips Res. Rep. 13 (1958) 1–9, https://doi.org/10.1142/9789814503464_0017.
[47] N. Tessier-Doyen, J.C. Glandus, M. Huger, Experimental and numerical study of elastic behaviour of heterogeneous model materials with spherical inclusions, J. Mater. Sci. 42 (2007) 5826–5834, https://doi.org/10.1007/s10853-006-1386-8.
[48] M.A. Schiavon, C. Gervais, F. Babonneau, G.D. Soraru, Crystallization behavior of novel silicon oxycarbide glasses, J. Am. Ceram. Soc. 87 (2008) 203–208, https://doi.org/10.1111/j.1551-2916.2004.00203.x.
[49] A.H. Tavakoli, P. Gerstel, J.A. Golczewski, J. Bill, Effect of boron on the crystallization of amorphous Si-(B-)C-N polymer-derived ceramics, J. Non-Cryst. Solids 355 (2009) 2381–2389, https://doi.org/10.1016/j.jnoncrysol.2009.08.010.
[50] D. Li, Z. Yang, D. Jia, X. Duan, Y. Zhou, D. Yu, Y. Tian, Z. Wang, Y. Liu, Role of boron addition on phase composition, microstructural evolution and mechanical properties of nanocrystalline SiBCN monoliths, J. Eur. Ceram. Soc. 38 (2018) 1179–1189, https://doi.org/10.1016/j.jeurceramsoc.2017.11.054.
[51] Z. Li, W. Zhou, X. Su, F. Luo, Y. Huang, C. Wang, Effect of boron doping on microwave dielectric properties of SiC powder synthesized by combustion synth-esis, J. Alloys Compd. 509 (2011) 973–976, https://doi.org/10.1016/j.jallcom. 2010.08.156.
[52] M. Gadzira, G. Gnesin, O. Mykhaylyk, O. Andreyev, Synthesis and structural peculiarities of non-stoichiometric beta-SiC, Diamond Relat. Mater. 7 (1998) 1466–1470, https://doi.org/10.1016/S0925-9635(98)00201-5.
[53] C.E. Lowell, Solid solution of boron in graphite, J. Am. Ceram. Soc. 50 (1967) 142–144, https://doi.org/10.1111/j.1151-2916.1967.tb15064.x.
[54] L.E. Jones, P.A. Thrower, Influence of boron on carbon fiber microstructure, phy-sical properties, and oxidation behavior, Carbon 29 (1991), https://doi.org/10. 1016/0008-6223(91)90076-U 251-169.
[55] M. Wieligor, Y. Wang, T.W. Zerda, Raman spectra of silicon carbide small particles and nanowires, J. Phys. Condens. Matter 17 (2005) 2387–2395, https://doi.org/10. 1088/0953-8984/17/15/010.
[56] C. Fantini, M.A. Pimenta, M.S. Strano, Two-phonon combination raman modes in covalently functionalized single-wall carbon nanotubes, J. Phys. Chem. C 112 (2008) 13150–13155, https://doi.org/10.1021/jp803855z.
[57] G. Mera, A. Tamayo, H. Nguyen, S. Sen, R. Riedel, Nanodomain structure of carbon-rRich silicon carbonitride polymer-derived ceramics, J. Am. Ceram. Soc. 93 (2010) 1169–1175, https://doi.org/10.1111/j.1551-2916.2009.03558.x.
[58] G. Mera, A. Navrotsky, S. Sen, H.J. Kleebe, R. Riedel, Polymer-derived SiCN and SiOC ceramics – structure and energetics at the nanoscale, J. Mater. Chem. A 1 (2013) 3826–3836, https://doi.org/10.1039/C2TA00727D.
[59] P. Venezuela, M. Lazzeri, F. Mauri, Theory of double-resonant Raman spectra in graphene: intensity and line shape of defect-induced and two-phonon bands, Phys. Rev. B 84 (2011) 035433, , https://doi.org/10.1103/PhysRevB.84.035433.
[60] A.C. Ferrari, Raman spectroscopy of graphene and graphite: disorder, electro-n–phonon coupling, doping and nonadiabatic effects, Solid State Comm. 143 (2007) 47–57, https://doi.org/10.1016/j.ssc.2007.03.052.
[61] Z. Li, A. Ghosh, A.S. Kobayashi, R.C. Bradt, Indentation fracture toughness of sin-tered silicon carbide in the Palmqvist crack regime, J. Am. Ceram. Soc. 7 (1989) 904–911, https://doi.org/10.1111/j.1151-2916.1989.tb06242.x.
[62] A. Ghosh, M.G. Jenkins, K.W. White, A.S. Kobayashi, R.C. Bradt, Elevated-temperature fracture resistance of a sintered α-silicon carbide, J. Am. Ceram. Soc. 72 (1989) 242, https://doi.org/10.1111/j.1151-2916.1989.tb06108.x.
[63] R.W. Rice, C. Wu, F. Borchelt, Hardness-grain size relations in ceramics, J. Am. Ceram. Soc. 77 (1994) 2539–2553, https://doi.org/10.1111/j.1151-2916.1994.tb04641.x.
[64] E.O. Hall, The deformation and ageing of mild steel.3. Discussion of results, Proc. Phys. Soc., Sect. B 64 (1951) 747–753, https://doi.org/10.1088/0370-1301/64/9/ 303.
[65] N.J. Petch, The cleavage strength of polycrystals, J. Iron Steel Inst. 174 (1953) 25–28, https://doi.org/10.1016/0013-7944(87)90050-6.
[66] B. Roman-Manso, E. Domingues, F.M. Figueiredo, M. Belmonte, P. Miranzo, Enhanced electrical conductivity of silicon carbide ceramics by addition of gra-phene nanoplatelets, J. Eur. Ceram. Soc. 35 (2015) 2723–2731, https://doi.org/10.1016/j.jeurceramsoc.2015.03.044.
[67] Y. Tajima, W.D. Kingery, Solid solubility of aluminum and boron in silicon carbide, J. Am. Ceram. Soc. 65 (1982) C27–C29, https://doi.org/10.1111/j.1151-2916.1982.tb10375.x.
[68] B. Matovic, G. Rixecker, J. Golczewski, F. Aldinger, Thermal conductivity of pressureless sintered silicon nitride materials with $LiYO_2$ additive, Sci. Sinter 36 (2004) 3–9, https://doi.org/10.2298/SOS0401003M.